Available online at www.sciencedirect.com
SCIENCE DIRECT®
International Journal of Plasticity 20 (2004) 2007–2026
INTERNATIONAL JOURNAL OF Plasticity
www.elsevier.com/locate/ijplas

A theory of compressive yield strength of nano-grained ceramics

B. Jiang, G.J. Weng *

Department of Mechanical and Aerospace Engineering, Rutgers University, New Brunswick, NJ 08903, USA

Received in final revised form 20 October 2003
Available online 26 April 2004

Dedicated to the memory of Daniel C. Drucker

Abstract

While most coarse-grained ceramics are brittle, nano-grained ceramics can exhibit significant ductility before failure. Such ductility is primarily contributed by the grain-boundary phase, but in grains of certain ceramic phase some plastic deformation has been found to occur and contribute to the overall plastic strain. In this paper a micromechanics-based composite model is developed to elucidate and predict the compressive yield strength of nano-grained ceramics as the grain size decreases from the coarse-grained to the nano-meter scale. The effects of porosity and second elastic phases are also considered. In such a multi-phase, porous, nano-grained ceramic, the collective behavior of all grains of a phase is represented by an elastoplastic constitutive equation, while the relative atomic sliding inside the grain boundary as observed in recent molecular dynamic simulations is represented by Drucker's [Q. Appl. Math. 7 (1950) 411] pressure-dependent plasticity theory. The average stress and strain state of the collective grains of each phase and the grain boundary, as well as the strain of the pores, are determined by the generalized self-consistent scheme and the direct self-consistent scheme, respectively, in conjunction with the secant-moduli approach. Applications of the developed theory to a TiO_2 indicated that the Hall–Petch plot, i.e., the compressive yield strength vs. $d^{-1/2}$ relation, showed a positive slope, but the slope continued to decrease, and eventually turned negative. Porosity can significantly lower the compressive yield stress, but it does not alter the fundament characteristics of its grain-size dependence. Second elastic phase can also have a significant effect on the yield strength of a nano-ceramic composite even at 10% of volume concentration.

* Corresponding author. Tel.: +1-732-445-2223; fax: +1-732-445-3124.
E-mail address: weng@jove.rutgers.edu (G.J. Weng).

0749-6419/$ - see front matter © 2004 Elsevier Ltd. All rights reserved.
doi:10.1016/j.ijplas.2003.10.010

Keywords: Nano-grained ceramics; Compressive yield strength; Generalized self-consistent method; Secant moduli; Micromechanics

1. Introduction

Nano-grained ceramics have their unique mechanical characteristics that are not commonly found in their coarse-grained counterparts. One of the most remarkable features is that they can exhibit low-temperature ductility. Karch et al. (1987) first reported that, with nano grain size, a brittle ceramic could permit a large plastic strain up to 100%. They observed that bending a notched nano-TiO_2 with an average grain size of about 8 nm would lead to crack opening, not immediate crack propagation that is characteristic of brittle fracture. Indentation of the same nano-TiO_2 also exhibited a large increase in indentation area, indicating plastic deformation at low temperature. For the same indentation on a coarse-grained TiO_2, it would have led to multiple cracking that is again typical of brittle characteristics. The nanocrystalline TiO_2 with the rutile structure produced by Hahn and Averback (1991) also exhibited ductile creep behavior between 600 and 800 °C. In these creep tests, however, grain size was found to grow from the initial 40 nm to the final values in the range of 120–1000 nm. In order for nano-grained ceramics to have benefits for structural applications, grain growth needs to be suppressed. Recently Kim et al. (2001) synthesized a 3-phase nano-ceramic composite consisting of 40 vol.% ZrO_2, 30 vol.% spinel ($MgAl_2O_4$), and 30 vol.% Al_2O_3, and found that, with such a multiphase composition, grain size remained stable in their tensile test at 1650 °C. They further demonstrated that, under the constant strain-rate loading of $\dot{\varepsilon} = 0.4\ s^{-1}$, their tensile specimen – with an average grain size of about 210 nm – could deform up to 1,050% without failure. In a separate investigation on the grain-size dependence of TiO_2 hardness, Höfler and Averback (1990), Guermazi et al. (1991), and Averback et al. (1992) reported a significant departure as the grain size decreased from the coarse grain to the nanometer range. They observed that, in the coarse-grained TiO_2 (above 0.4 μm), the hardness vs. grain size scaled well with the Hall–Petch relation. This prompted them to suggest that there could be dislocation activity in the coarse grains (our later calculations confirmed their conjecture), but probably not in the nano-sized grains. They further reported that porosity could significantly reduce the hardness of the nano-grained TiO_2. As hardness could be scaled with the compressive yield strength by a factor of 3 (Tabor, 1951; McClintock and Argon, 1966), one could conclude that both porosity and grain-size are two critical factors affecting the hardness and compressive yield strength of nano-grained ceramics.

Nano-grained materials are commonly referred to as the class of materials whose average grain size is less than several tens of nano-meters. Since Birringer et al. (1984) first reported that it was possible to combine the method of inert gas condensation of small particles with in situ powder compaction to synthesize materials with grain sizes of 5–15 nm, considerable progress has been made in this field. Karch et al. (1987) originally explained the increased ductility observed in a nano-TiO_2 on the basis of

Coble creep, under which the creep rate $\dot{\varepsilon}$ depends on the grain size d as $\dot{\varepsilon} \sim d^{-3}$. Thus if the grain size decreases from 10 μm to 10 nm, the creep rate would have increased by 10^9, making an otherwise brittle material ductile (Their reasoning is now not the only one to explain the superplastic behavior of nano-grained materials). Subsequently several tests have been conducted on nanocrystalline metals. The most conspicuous characteristic out of the measurements of Cu and Pd is that, in the coarse-grain range, the hardness (or yield strength) increased linearly with $d^{-1/2}$, but as the grain size decreased to the nano-meter range, a negative slope was observed (Chokshi et al., 1989). The transition from a positive slope to a negative one was further substantiated by the experiments of Lu et al. (1990) on Ni–P alloy, and Fougere et al. (1992) also on Cu and Pd. These tests point to the existence of an optimal grain size in the nano-meter range that the material would possess the strongest hardness and highest compressive yield strength. While early processing was often accompanied by various voids and defects, subsequent improvement in processing technique has produced specimen with a higher hardness but nonetheless still displayed the same observed negative slope in the Hall–Petch plot (see, for instance, Sanders et al., 1997a,b, Weertman et al., 1999, and papers in the Julia R. Weertman Symposium, 1999).

In addition to porosity and grain size, another important factor that can affect the compressive strength of a nanocrystalline ceramic – in light of the composite structure of Kim et al. (2001) – is the presence of second elastic phases. The mixing and compaction technique developed by them required the nano-ceramic to be in the form of a multi-phase composite. The composite structure was crucial for the nano-ceramic to exhibit high strain-rate (up to 1 s^{-1}) ductility without significant grain growth. To address these factors, we will develop a micromechanics model that can account for the influence of porosity, grain size, and multiphase, on the yield strength of nano-grained ceramics. The developed theory will be compared with the measured TiO_2 strength. In this study we will be mainly concerned with the compressive yield stress defined around 0.2% of proof strain, and the stress–strain behavior within the small strain range. Therefore large deformation that is essential for the study of super-plasticity with an elongation up to tens or hundreds, or even thousands of percents as demonstrated in the high strain-rate, high temperature test of Kim et al. on Cu, will not be included. Such a study would require a finite-deformation formulation for which no appropriate micromechanics formulae are yet available to account for the evolution of stress field and microstructural changes. Within this objective, the grain-boundary sliding often reported to be essential to superplastic flow could be accounted for by the plastic deformation of the finite thickness, grain-boundary phase of the model. Even though no superplasticity will be calculated, the model will give results regarding the yet-unknown characteristics of a nano-ceramic composite and provide some insights into the compositional dependence of its mechanical strength.

2. A nano-grained ceramic model with porosity and multiphase

While it has been known for over a decade that, in a nanocrystalline solid, a significant portion of atoms reside in the grain boundary regions, it is the recent

molecular dynamic simulations (e.g. Schiøtz et al., 1998, 1999; Van Swygenhoven et al., 1999; Yamakov et al., 2002) that inspired us to develop a micromechanical model to mimic the microstructure of such a material. A representative one from Schiøtz et al. (1998) for a nanocrystalline copper using 100,000 atoms is reproduced in Fig. 1(a); it

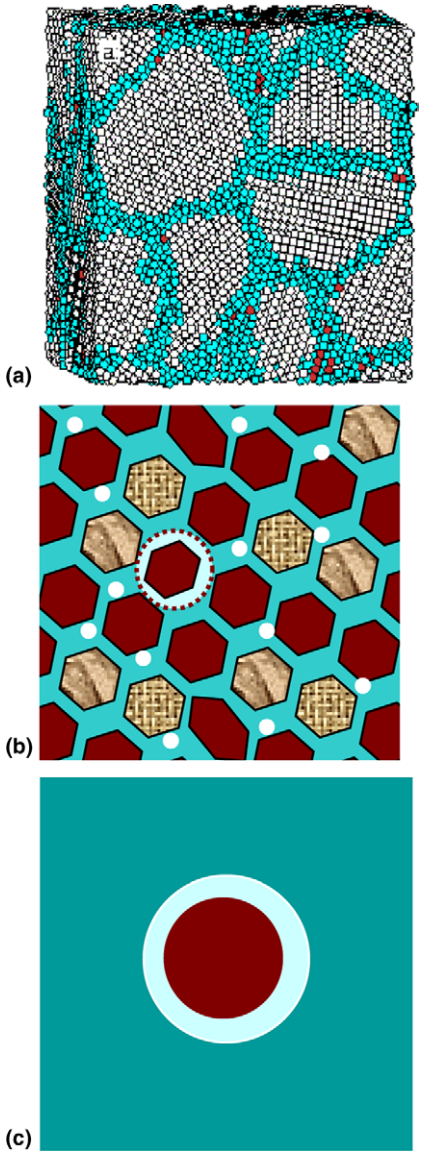

Fig. 1. (a) Molecular dynamic simulation of grains and grain boundary in a nano-grained copper, showing the grain boundary has finite volume concentration, (b) a schematic diagram of a porous, multiphase, nano-grained ceramic, and (c) the generalized self-consistent model.

shows that, unlike in traditional coarse-grained materials, the grain boundary now constitutes a distinct phase with finite thickness and possesses certain volume fraction. Hydrogen probe of grain-boundary thickness suggested that it has the value of about 0.5–1.5 nm (Mütschele and Kirchheim, 1987; Kirchheim et al., 1988), and atomic simulations indicated that it is not sensitive to the grain size (Schiøtz, 2003). Such a nanocrystalline solid can be construed as a two-phase material consisting of the grains and the grain-boundary phase, which has served as the basis of our recent model for nanocrystalline metals (Jiang and Weng, 2003). Denoting d as the average grain size and δ as the grain-boundary thickness, the volume concentration (fraction) of the grains can be approximated by

$$c_{\mathrm{g}} = \left(\frac{d}{d+\delta}\right)^3, \tag{2.1}$$

and that of the grain boundary by $c_{\mathrm{gb}} = 1 - c_{\mathrm{g}}$. The significance of grain-boundary phase in the nanocrystalline solid is then evident. For instance, at the average grain size of $d = 25$ nm and grain-boundary thickness $\delta = 1$ nm, the grain boundary occupies about 11% of the material, and at $d = 10$ nm it takes about 25%. As such, its plastic deformation due to the relative, uncorrelated, atomic motion uncovered in molecular dynamic simulations (Schiøtz et al., 1998, 1999) can contribute significantly to the overall plastic strain of the nanocrystalline solid.

For the study of nano-grained ceramics with porosity and possible multiphase, we envision a microstructure as depicted in Fig. 1(b). Here three types of phases (i.e., such as the ZrO_2–spinel–Al_2O_3 composite of Kim et al., 2001) are depicted, along with pores signified by the white dots. If the porosity of the ceramic is denoted by c_{pore}, then the total volume fraction of all phase grains, denoted by c_{g}, and that of the grain-boundary phase, c_{gb}, can be approximately represented as

$$c_{\mathrm{g}} = (1 - c_{\mathrm{pore}})\left(\frac{d}{d+\delta}\right)^3, \qquad c_{\mathrm{gb}} = (1 - c_{\mathrm{pore}})\left[1 - \left(\frac{d}{d+\delta}\right)^3\right], \tag{2.2}$$

where $c_{\mathrm{g}} = \sum_{k=1}^{N} c_{\mathrm{g}}^{(k)}$, is the sum of the volume fractions of all phase grains, $c_{\mathrm{g}}^{(k)}$. Denoting $f_{(k)}$ as the fraction of the kth phase in all phases, we also note

$$c_{\mathrm{g}}^{(k)} = f_{(k)} c_{\mathrm{g}}, \quad \sum_{k=1}^{N} f_{(k)} = 1, \quad \text{and} \quad \sum_{k=1}^{N} c_{\mathrm{g}}^{(k)} + c_{\mathrm{gb}} + c_{\mathrm{pore}} = 1. \tag{2.3}$$

When there is only a single phase without any porosity, this recovers the model of (2.1). Here for simplicity the grain sizes of all phases are taken to be about the same, but if significantly different, c_{g} would have to be constructed anew.

3. Constitutive equations of the individual phases and the grain boundary

Plastic deformation in coarse-grained materials generally occur by dislocation motion or diffusional creep in the constituent grains. Dislocation density and mobility in most ceramics, however, are usually limited and only in certain types of

ceramics has such deformation been observed. For instance in the 3-phase nano-ceramic composite synthesized by Kim et al. (2001), dislocation structures are reported only in ZrO_2 grains. In order to pave the way for the study of coarse-to-nano grain transition, however, the constitutive equations of the grains will be written in the way of capable of undergoing plastic deformation. Grains, which deform only elastically, then can be viewed as a material with an extremely high yield stress. An elastic-plastic constitutive equation is particularly essential in light of the TiO_2 results reported by Averback et al. (1992), who strongly suggested that dislocations might play a role for the rapid decrease of hardness in the coarse grain range.

3.1. Constitutive equations of the collective grains of an individual phase

In the multiphase, porous ceramic with a finite grain-boundary thickness as depicted in Fig. 1(b), the collective stress–strain behavior of all constituent grains of a particular phase is isotropic, and will be represented by a constitutive equation in terms of von Mises' effective stress and strain. According to an earlier study on the grain-size dependence of yield strength of coarse-grained polycrystals (Weng, 1983), the resolved shear stress–shear strain relation of a slip system in the constituent grain is grain-size dependent due to the possible dislocation pile-ups and the dislocation substructures affected by the grain boundary, and such a dependence necessarily translates into the level of overall polycrystal. This suggests that the stress–strain relation of the collective grains of each individual phase is also grain-size dependent. In general the effective stress–strain relation of the collective grains of a phase can be written as

$$\sigma_{\mathrm{e}} = \sigma_{\mathrm{y}}^{(\mathrm{g})} + h_{\mathrm{g}} \cdot \left(\varepsilon_{\mathrm{e}}^{\mathrm{p}}\right)^{n_{\mathrm{g}}}, \tag{3.1}$$

where σ_{e} is von Mises' effective stress and $\varepsilon_{\mathrm{e}}^{\mathrm{p}}$ the effective plastic strain, defined by

$$\sigma_{\mathrm{e}} = \left(\frac{3}{2}\sigma'_{ij}\sigma'_{ij}\right)^{1/2}, \qquad \varepsilon_{\mathrm{e}}^{\mathrm{p}} = \left(\frac{2}{3}\varepsilon_{ij}^{\mathrm{p}}\varepsilon_{ij}^{\mathrm{p}}\right)^{1/2}, \tag{3.2}$$

in terms of the deviatoric stress σ'_{ij} and plastic strain $\varepsilon_{ij}^{\mathrm{p}}$. Here $\sigma_{\mathrm{y}}^{(\mathrm{g})}$, h_{g} and n_{g} are respectively the initial yield stress, strength coefficient, and work hardening exponent. Both σ_{y} and h now depend on the grain size d in the form of Hall–Petch relation

$$\sigma_{\mathrm{y}}^{(\mathrm{g})} = \sigma_{\mathrm{y}}^{\infty(g)} + k \cdot d^{-\frac{1}{2}}, \qquad h_{\mathrm{g}} = h_{\mathrm{g}}^{\infty} + a \cdot d^{-\frac{1}{2}}, \tag{3.3}$$

where $\sigma_{\mathrm{y}}^{\infty(g)}$, k, h_{g}^{∞}, and a are material constants, corresponding to grains of infinite size or single crystals. To describe the elastic response, the bulk and shear moduli of the collective grains of a phase will be denoted by κ_{g} and μ_{g}, and Young's modulus and Poisson's ratio by E_{g} and ν_{g}, respectively. In a multiphase ceramic each phase will of course have its own material constants.

To pave the way for later determination of compressive yield stress of the multiphase porous ceramic, it is useful to note that, at a given level of effective stress σ_{e} or effective plastic strain $\varepsilon_{\mathrm{e}}^{\mathrm{p}}$, the secant Young's modulus (defined as the ratio of stress to total strain) and secant Poisson's ratio are given by

$$E_{\mathrm{g}}^{\mathrm{s}}=\frac{1}{\dfrac{1}{E_{\mathrm{g}}}+\dfrac{\varepsilon_{\mathrm{e}}^{\mathrm{p}(g)}}{\sigma_{\mathrm{e}}^{(\mathrm{g})}}},\qquad \nu_{\mathrm{g}}^{\mathrm{s}}=\frac{1}{2}-\left(\frac{1}{2}-\nu_{\mathrm{g}}\right)\frac{E_{\mathrm{g}}^{\mathrm{s}}}{E_{\mathrm{g}}},\tag{3.4}$$

whereas the secant bulk and shear moduli follow from the isotropic relations

$$\kappa_{\mathrm{g}}^{\mathrm{s}}=\frac{E_{\mathrm{g}}^{\mathrm{s}}}{3(1-2\nu_{\mathrm{g}}^{\mathrm{s}})},\qquad \mu_{\mathrm{g}}^{\mathrm{s}}=\frac{E_{\mathrm{g}}^{\mathrm{s}}}{2(1+\nu_{\mathrm{g}}^{\mathrm{s}})}.\tag{3.5}$$

3.2. Constitutive equations of the grain boundary

As revealed by various atomic simulations (see, for instance, Schiøtz et al., 1998, 1999; Van Swygenhoven et al., 1999; Gleiter, 2000), the atomic structure of the grain-boundary regions is mostly amorphous. This implies that its plastic behavior cannot be represented by von Mises' effective stress and strain alone. The study by Schiøtz et al. (1998, 1999) on copper further disclosed that plastic deformation inside the grain boundary occurred by atomic sliding through a large number of uncorrelated events, where a few atoms (or a few tens of atoms) slide with respect to each other. To describe such a plastic behavior for the amorphous grain-boundary phase by a continuum model, we invoke Drucker's (1950) constitutive equation, which has also proven suitable for the modeling of metallic glasses (Donovan, 1989). Drucker's equation is marked by the pressure dependence of the yield stress; it can be written as

$$\sigma_{\mathrm{e}}=\sigma_{\mathrm{y}}^{(\mathrm{gb})}+m\cdot p+h_{\mathrm{gb}}\cdot\left(\varepsilon_{\mathrm{e}}^{\mathrm{p}}\right)^{n_{\mathrm{gb}}},\tag{3.6}$$

where $p=-\frac{1}{3}\sigma_{kk}$ is the hydrostatic pressure, and $\sigma_{\mathrm{y}}^{(\mathrm{gb})}, m, h_{\mathrm{gb}}$, and n_{gb} are material constants of the grain-boundary phase. Its elastic moduli will be written with the subscript 'gb', and so will its secant moduli, which could also be cast in a form similar to Eqs. (3.4) and (3.5).

4. Stress and strain state, and stress–strain relation of a porous, multiphase, nano-grained ceramic

The microstructure as depicted in Fig. 1(b) accounts for the simultaneous presence of several phases and porosity in a nano-grained ceramic that possesses a finite grain-boundary thickness. These microstructural features are represented by the grain size d, the grain-boundary thickness δ, and the volume concentrations of the individual phases $c_{\mathrm{g}}^{(k)}$, c_{gb} and c_{pore}. In order to evaluate the overall property of such a composite system, the stress and strain state of each individual phase will have to be determined first.

To this end we shall follow the approach taken by our earlier study on a single-phase nanocrystalline metal without any porosity, and treat the stress and strain state of collective grains of a particular phase by the generalized self-consistent scheme (Christensen and Lo, 1979). Such a scheme is particularly suited for high volume concentration and is depicted in Fig. 1(c) in light of the schematic diagram of Fig. 1(b). The spherical inclusion – with an elastoplastic property represented by

Eqs. (3.1)–(3.5) of the behavior of collective grains of a particular phase – is now embedded in the grain-boundary phase (represented by the white shell), which is further embedded in an infinitely effective medium with the yet-unknown overall property of the multi-phase, porous ceramic. Such an embedding process is repeated for each and every phase so that the stress and strain state of each phase grains can be established (see also Huang et al., 1994). The strain state of the pores will be determined by the direct self-consistent scheme (Hill, 1965b; Budiansky, 1995) by embedding it in the effective medium. We do not treat pores on equal footing with grains here because grains are always surrounded by grain boundary, but pores – which tend to exist at the triple junction points of grains during the compaction process of ceramics – may be surrounded simultaneously by both grain boundary and grains. Even though the presence of pores is significant, the porosity in real ceramics in not high enough to cause the breakdown of the self-consistent scheme commonly associated with the voided or cracked problem. Thus the average stress and strain state of all phase grains and pores are all expressed in terms of those of the overall effective medium, their respective secant moduli, and the volume concentrations $c_{\mathrm{g}}^{(k)}$, c_{gb} and c_{pore}. Under a given external stress, the overall strain of the composite is then calculated from the weighted mean of the strains of all phases. The overall stress–strain relation of the multiphase, porous ceramic then can be established.

The nonlinear elastoplastic problem of the composite will be addressed by a linear approach by way of secant moduli. Since its inception in Talbot and Willis (1985), this method has seen its growth in several forms with various degrees of sophistication (e.g. Tandon and Weng, 1988; Ponte Castañeda, 1991; Willis, 1991; Qiu and Weng, 1992; Suquet, 1995; Hu, 1996). Here we shall not dwell upon the rigor of each individual approach but instead concentrate on the physical problem of ceramic strength. For this reason and also for the fact that several different constituent phases are involved here, we shall adopt the direct approach of Tandon and Weng (1988), which was inspired by Berveiller and Zaoui's (1979) modification of Hill's (1965a) original incremental scheme.

4.1. Average stress and strain in the grains, grain boundary, and pores

Within the linear context, such a procedure has a well-known solution from Christensen and Lo's formulation. After some algebra, their local solution can be used to find the average stress and strain of the grain (inclusion) and grain boundary (matrix), now in terms of the secant moduli of the constituent phases, as

$$\begin{aligned}
\bar{\sigma}_{ij}^{(\mathrm{g})} &= \frac{1}{3}\bar{\alpha}_{\mathrm{g}}\bar{\sigma}_{kk}\delta_{ij} + \bar{\beta}_{\mathrm{g}}\bar{\sigma}'_{ij}, \qquad \bar{\varepsilon}_{ij}^{(\mathrm{g})} = \frac{\bar{\alpha}_{\mathrm{g}}}{9\kappa_{\mathrm{g}}^{\mathrm{s}}}\bar{\sigma}_{kk}\delta_{ij} + \frac{\bar{\beta}_{\mathrm{g}}}{2\mu_{\mathrm{g}}^{\mathrm{s}}}\cdot\bar{\sigma}'_{ij}, \\
\bar{\sigma}_{ij}^{(\mathrm{gb})} &= \frac{1}{3}\bar{\alpha}_{\mathrm{gb}}\bar{\sigma}_{kk}\delta_{ij} + \bar{\beta}_{\mathrm{gb}}\bar{\sigma}'_{ij}, \qquad \bar{\varepsilon}_{ij}^{(\mathrm{gb})} = \frac{\bar{\alpha}_{\mathrm{gb}}}{9\kappa_{\mathrm{gb}}^{\mathrm{s}}}\bar{\sigma}_{kk}\delta_{ij} + \frac{\bar{\beta}_{\mathrm{gb}}}{2\mu_{\mathrm{gb}}^{\mathrm{s}}}\cdot\bar{\sigma}'_{ij},
\end{aligned} \tag{4.1}$$

where coefficients $\bar{\alpha}_{\mathrm{g}}$, $\bar{\alpha}_{\mathrm{gb}}$, $\bar{\beta}_{\mathrm{g}}$ and $\bar{\beta}_{\mathrm{gb}}$ relate the average hydrostatic and deviatoric stresses in the grains and grain-boundary phase to the externally applied $(\bar{\sigma}_{kk}, \bar{\sigma}'_{ij})$ (Note: an overbar signifies that it is a volume-averaged quantity). We found that

$$
\begin{aligned}
\bar{\alpha}_{\mathrm{g}} &= \frac{1}{p}(3\kappa_{\mathrm{c}}^{\mathrm{s}} + 4\mu_{\mathrm{c}}^{\mathrm{s}})(3\kappa_{\mathrm{gb}}^{\mathrm{s}} + 4\mu_{\mathrm{gb}}^{\mathrm{s}})\frac{\kappa_{\mathrm{g}}^{\mathrm{s}}}{\kappa_{\mathrm{c}}^{\mathrm{s}}},\\
\bar{\beta}_{\mathrm{g}} &= 2\mu_{\mathrm{g}}^{\mathrm{s}}\left[\bar{a}_1 - \frac{21}{5(1-2\nu_{\mathrm{g}})}\bar{a}_2\right],\\
\bar{\alpha}_{\mathrm{gb}} &= \frac{1}{p}(3\kappa_{\mathrm{c}}^{\mathrm{s}} + 4\mu_{\mathrm{c}}^{\mathrm{s}})(3\kappa_{\mathrm{g}} + 4\mu_{\mathrm{gb}}^{\mathrm{s}})\frac{\kappa_{\mathrm{gb}}^{\mathrm{s}}}{\kappa_{\mathrm{c}}^{\mathrm{s}}},\\
\bar{\beta}_{\mathrm{gb}} &= 2\mu_{\mathrm{gb}}^{\mathrm{s}}\left[\bar{b}_1 - \frac{21}{5(1-2\nu_{\mathrm{gb}}^{\mathrm{s}})}\frac{1-c_{\mathrm{g}}^{5/3}}{1-c_{\mathrm{g}}}\bar{b}_2\right]
\end{aligned}
\tag{4.2}
$$

and

$$
p = (3\kappa_{\mathrm{g}} + 4\mu_{\mathrm{gb}}^{\mathrm{s}})(3\kappa_{\mathrm{gb}}^{\mathrm{s}} + 4\mu_{\mathrm{c}}^{\mathrm{s}}) - 12c_{\mathrm{g}}(\kappa_{\mathrm{g}} - \kappa_{\mathrm{gb}}^{\mathrm{s}})(\mu_{\mathrm{c}}^{\mathrm{s}} - \mu_{\mathrm{gb}}^{\mathrm{s}}), \tag{4.3}
$$

where $(\kappa_{\mathrm{c}}^{\mathrm{s}}, \mu_{\mathrm{c}}^{\mathrm{s}})$ are the secant bulk and shear moduli of the composite (including multi phases, grain boundary, and pores) at the considered level of applied stress $\bar{\sigma}_{ij}$. The constants $\bar{a}_1$, $\bar{a}_2$, $\bar{b}_1$ and $\bar{b}_2$ are given in the Appendix A. It should be noted that, in a multiphase ceramic, the values of the $(\kappa_{\mathrm{g}}, \mu_{\mathrm{g}}^{\mathrm{s}})$ pair correspond to those of a considered phase, thereby giving rise to different average stress and strain in the inclusions of different phases.

For the pores, the average strain could be evaluated from the self-consistent scheme. Again in the context of secant moduli, Eshelby's solution (1957) readily provides

$$
\bar{\varepsilon}_{ij}^{(\mathrm{pore})} = \frac{\bar{\alpha}_{\mathrm{pore}}}{9\kappa_{\mathrm{c}}^{\mathrm{s}}}\bar{\sigma}_{kk}\delta_{ij} + \frac{\bar{\beta}_{\mathrm{pore}}}{2\mu_{\mathrm{c}}^{\mathrm{s}}}\bar{\sigma}'_{ij}, \tag{4.4}
$$

with

$$
\bar{\alpha}_{\mathrm{pore}} = \frac{3\kappa_{\mathrm{c}}^{\mathrm{s}} + 4\mu_{\mathrm{c}}^{\mathrm{s}}}{4\mu_{\mathrm{c}}^{\mathrm{s}}}, \qquad \bar{\beta}_{\mathrm{pore}} = \frac{5(3\kappa_{\mathrm{c}}^{\mathrm{s}} + 4\mu_{\mathrm{c}}^{\mathrm{s}})}{9\kappa_{\mathrm{c}}^{\mathrm{s}} + 8\mu_{\mathrm{c}}^{\mathrm{s}}}. \tag{4.5}
$$

As both $\kappa_{\mathrm{c}}^{\mathrm{s}}$ and $\mu_{\mathrm{c}}^{\mathrm{s}}$ are not yet known, these quantities need to be evaluated by an iterative procedure, to be described next.

4.2. The secant moduli of the porous, nano-grained, multi-phase ceramic

Once the secant bulk and shear moduli $(\kappa_{\mathrm{c}}^{\mathrm{s}}, \mu_{\mathrm{c}}^{\mathrm{s}})$ at a given level of applied stress $\bar{\sigma}_{ij}$, are known, the overall strain follows immediately. Then by increasing the level of applied stress, the entire stress–strain relation of the composite, and its compressive yield strength defined as the flow stress at 0.2% plastic strain, can be evaluated as a function of porosity and grain size. In the context of secant moduli under proportional loading, the constitutive relations of the composite can be written as

$$
\bar{\varepsilon}_{ij} = M_{ijkl}^{(\mathrm{c})\mathrm{s}}\bar{\sigma}_{kl}, \tag{4.6}
$$

where $M_{ijkl}^{(\mathrm{c})\mathrm{s}} = \left(\frac{1}{3\kappa_{\mathrm{c}}^{\mathrm{s}}}, \frac{1}{2\mu_{\mathrm{c}}^{\mathrm{s}}}\right)$ is its effective secant compliance tensor. From the weighted mean of the average strains of all constituent phases (grains, grain-boundary, and pores), the composite strain is given by

$$\bar{\varepsilon}_{ij} = \langle \varepsilon_{ij} \rangle = \sum_{k=1}^{N} c_{\mathrm{g}}^{(k)} \bar{\varepsilon}_{ij}^{(\mathrm{g})(k)} + c_{\mathrm{pore}} \bar{\varepsilon}_{ij}^{(\mathrm{pore})} + c_{\mathrm{gb}} \sum_{k=1}^{N} f_{(k)} \bar{\varepsilon}_{ij}^{(\mathrm{gb})(k)}, \tag{4.7}$$

where $\sum_{k=1}^{N} f_{(k)} \bar{\varepsilon}_{ij}^{(\mathrm{gb})(k)}$ – recalling the meaning of $f_{(k)}$ in (2.3) – is the weighted mean of $\bar{\varepsilon}_{ij}^{(\mathrm{gb})}$ values when different phases take the position of $(\kappa_{\mathrm{g}}, \mu_{\mathrm{g}}^{\mathrm{s}})$ in Eq. (4.1). Of course for a single-phase, nano-grained ceramic with certain amount of porosity as the TiO_2 to be discussed later, no such average is required.

Since the strains of all constituent phases are all expressed in terms of the applied stress $\bar{\sigma}_{ij}$, Eqs. (4.6) and (4.7) allow one to solve for the effective secant moduli, $(\kappa_{\mathrm{c}}^{\mathrm{s}}, \mu_{\mathrm{c}}^{\mathrm{s}})$, after canceling out the hydrostatic and deviatoric components of the applied stress on both sides, as

$$\begin{aligned} \frac{1}{\kappa_{\mathrm{c}}^{\mathrm{s}}} &= \sum_{k=1}^{N} c_{\mathrm{g}}^{(k)} \frac{\bar{\alpha}_{\mathrm{g}}^{(k)}}{\kappa_{\mathrm{g}}^{(k)}} + c_{\mathrm{pore}} \frac{\bar{\alpha}_{\mathrm{pore}}}{\kappa_{\mathrm{c}}^{\mathrm{s}}} + c_{\mathrm{gb}} \sum_{k=1}^{N} f_{(k)} \frac{\bar{\alpha}_{\mathrm{gb}}^{(k)}}{\kappa_{\mathrm{gb}}^{\mathrm{s}(k)}}, \\ \frac{1}{\mu_{\mathrm{c}}^{\mathrm{s}}} &= \sum_{k=1}^{N} c_{\mathrm{g}}^{(k)} \frac{\bar{\beta}_{\mathrm{g}}^{(k)}}{\mu_{\mathrm{g}}^{\mathrm{s}(k)}} + c_{\mathrm{pore}} \frac{\bar{\beta}_{\mathrm{pore}}}{\mu_{\mathrm{c}}^{\mathrm{s}}} + c_{\mathrm{gb}} \sum_{k=1}^{N} f_{(k)} \frac{\bar{\beta}_{\mathrm{gb}}^{(k)}}{\mu_{\mathrm{gb}}^{\mathrm{s}(k)}}. \end{aligned} \tag{4.8}$$

It should be pointed out that Christensen and Lo's (1979) effective bulk and shear moduli do not give the present results involving several constituent phases and porosity; it is only under the condition that, when $c_{\mathrm{pore}} = 0$ and $N = 1$, their bulk and shear moduli could be used here.

4.3. Computational procedure

The pair in Eq. (4.8) can be used to solve for the effective secant bulk and shear moduli. Since parameters $\bar{\alpha}_{\mathrm{g}}$, $\bar{\alpha}_{\mathrm{gb}}$, $\bar{\beta}_{\mathrm{g}}$, $\bar{\beta}_{\mathrm{gb}}$, $\bar{\alpha}_{\mathrm{pore}}$ and $\bar{\beta}_{\mathrm{pore}}$ also depend on $\kappa_{\mathrm{c}}^{\mathrm{s}}$ and $\mu_{\mathrm{c}}^{\mathrm{s}}$, an iteration scheme is required here. Briefly we first assumed a set of secant bulk and shear moduli of the composite and constituent phases to calculate the parameters $\bar{\alpha}_{\mathrm{g}}$, $\bar{\alpha}_{\mathrm{gb}}$, $\bar{\beta}_{\mathrm{g}}$, $\bar{\beta}_{\mathrm{gb}}$, $\bar{\alpha}_{\mathrm{pore}}$ and $\bar{\beta}_{\mathrm{pore}}$. The local stresses in the grains and grain boundary calculated from (4.1) were then compared with their respective flow stresses in the constitutive Eqs. (3.1) and (3.6), to check for consistency. If no, the secant moduli of the grains and grain boundary were then determined from the constitutive equations. Then through Eq. (4.8), we determined the new secant bulk and shear moduli of the composite. These new secant moduli were then used to start a new round of iteration, until the calculated results of the composite and the constituent phases were sufficiently close to the assumed ones. Then by increasing the level of applied stress, the entire stress–strain curve and the compressive yield strength at 0.2% proof strain were determined.

5. Effects of porosity and grain size on the compressive yield strength of a nano-grained TiO_2

We now use the developed theory to examine the effects of porosity and grain size on the compressive yield strength of a nano-grained rutile TiO_2. Such a titanium

oxide has been processed and tested by Höfler and Averback (1990) and Averback et al. (1992), so their data could be compared with the theory.

But before we proceed to examine this ceramic, it is instructive to look at one of our recent calculations on the yield strength of Cu and an idealized material whose grains deform only elastically (Jiang and Weng, 2003). Such a result is reproduced in Fig. 2. This figure illustrates the 0.2% yield stress vs. $d^{-1/2}$ relation, or the Hall–Petch plot, over the grain-size range between 20 μm and 10 nm (see the top scale). The bottom curve connecting the diamond-shaped points was generated using the full elastoplastic properties of the collective Cu grains, whereas the top one connecting the open circles was obtained assuming the inclusions to be purely elastic (with the Cu elastic moduli). In both cases the plastic deformation of the grain-boundary phase was fully incorporated. The yield behavior of the real Cu (the bottom curve) is seen to follow the traditional Hall–Petch relation in the coarse-grained region, but as the grain size decreased to the nano-meter range it began to deviate, and eventually decreased. For the idealized system of elastic grains and elastoplastic grain boundary (the top curve), the Hall–Petch plot showed a continuous decrease of the slope, and the slope was always negative. The bottom and top curves eventually merged into a single one, during which, as reported in the original paper, the overall plastic behavior of the nano-crystalline solid was totally dominated by the grain-boundary phase and the plasticity of the grains played no role.

This figure is significant to the present study of ceramics, for if the grains of the ceramic were totally incapable of having plastic deformation, the Hall–Petch plot

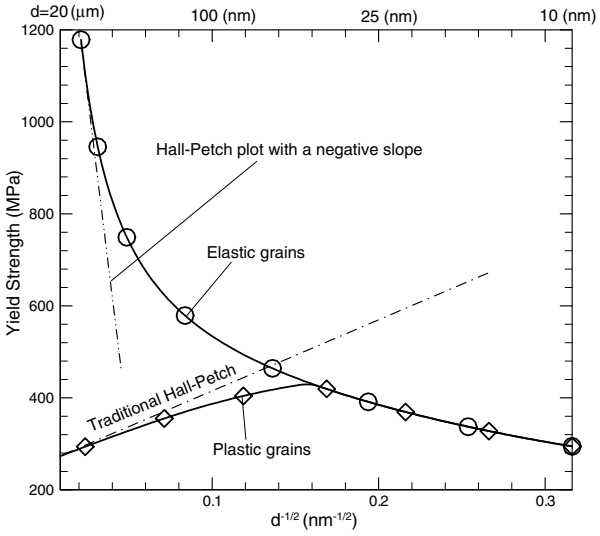

Fig. 2. The Hall–Petch plot of the yield stress vs. $d^{-1/2}$ relation as the grain size decreases from coarse grains to nano grains. The bottom curve was calculated with plastic grains whereas the top one was with elastic grains. Both curves eventually merge into a single one in the nano-meter range (Jiang and Weng, 2003).

would have displayed a similar trend as the top curve. The test data of Höfler and Averback (1990) and Averback et al. (1992), reproduced in Fig. 3 at two levels of porosity $c_{\text{pore}} = 6\%$ and 11%, however, clearly showed a positive slope. This is consistent with their belief that dislocations played a role in this TiO_2 grains. (These data were converted from their Vickers hardness tests by Tabor's relation). The increase of the compressive strength over the entire range of grain sizes was also not linear as the Hall–Petch relation would have implied. Clearly the slope is higher with coarse grains, and lower with nano grains, and this has prompted them to suggest a bilinear curve to represent these two segments of the data. Such a transition also reflects what we earlier concluded of a more and more dominant role of the grain boundary as the grain size enters into the nano-meter range. At a given grain size, their square-shaped data with 6% porosity indicated a substantially higher yield stress as compared to that of the triangular-shaped data with 12% porosity. The difference between the two was almost parallel, suggesting that pores played a consistent role of reducing the yield strength, but they did not alter the basic characteristics of the transition of the compressive yield strength, which was totally determined by the grain size.

Our theoretical calculations are plotted alongside using the material constants listed in Table 1. These theoretical results indicated that the strength increased nonlinearly with a decreasing slope, and then attained a maximum value at a critical grain size, after which it began to decrease with a negative slope. The optimal grain size occurs in the nanometer range between 10 and 25 nm. Within the range of grain sizes tested, these theoretical predictions appear to have captured the general trend

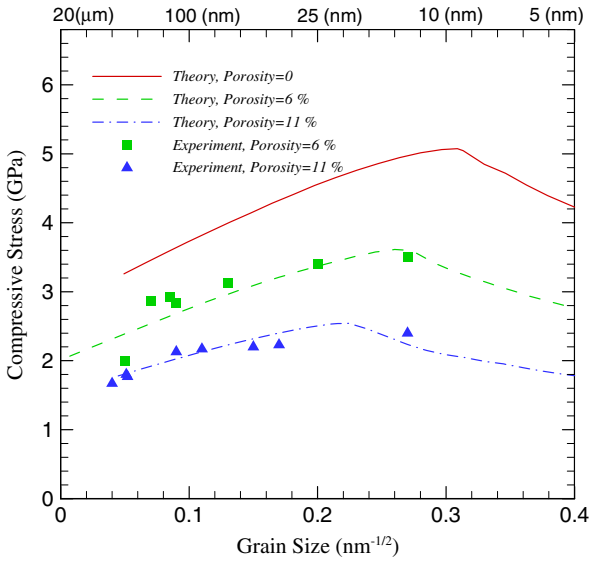

Fig. 3. Compressive yield stress as a function of grain size d at three levels of porosity (experimental data from Averback et al., 1992).

Table 1
Material parameters used in calculations

	Grains	Grain boundary
E (GPa)	281.0	260.67
v	0.28	0.28
σ_y (GPa)	1.85	1.0
h (GPa)	6.88	6.2
n	0.5	0.4
k (GPa$\sqrt{\text{nm}}$)	8.0	–
a (GPa$\sqrt{\text{nm}}$)	0.243	–
m	–	1.0

of the data. This further substantiates their conjecture that dislocation mechanism had indeed played a role in the grains.

Since there was only one experimental data after the turn of the slope, it is not clear whether a negative slope would have been observed had they extended their tests to grain sizes below 10 nm. The existence of such a critical grain size – called critical equicohesive grain size – has been observed by Chokshi et al. (1989) and Sanders et al. (1997a,b) on Cu and Pd, and also predicted by our recent theory for nanocrystalline metals (Jiang and Weng, 2003). It stemmed from the softer yield strength of the grain-boundary phase as compared to the grains. Theoretically it can be visualized that, if the grain-boundary phase is softer than the grains, then as the grain size approaches zero the yield strength of the nanocrystalline material would asymptotically approach that of the grain boundary, which is represented by the end points of the plot as the abscissa extends to infinity. So if the grain boundary is substantially softer than the grains, then a negative slope will eventually appear, but if it were harder than the grains then the slope would continue to remain positive, in fact increasing. Whether such a critical grain size could be observed for this TiO_2 or other ceramics as in nanocrystalline metals remains an open challenge.

Our calculations also show that the effect of porosity is significant. Porosity moved the curves almost vertically in parallel fashion. This demonstrates again that porosity only alters the magnitude of the hardness or compressive yield strength, but it does not change the basic characteristics of the transition of yield strength as the grain size decreases from the coarse-grained to the nano-grained regime. Our calculations further show that the critical grain size increases with porosity.

Even though perfectly dense TiO_2 was difficult to synthesize, it is possible to make a theoretical calculation. The solid line in this figure was obtained by setting the porosity to zero; the result was a higher compressive yield stress at the same grain size. The difference between the results of 0% and 6% porosity, and that of 6% and 11% porosity, are seen to be about proportional. This characteristic is consistent with the decrease of Young's modulus and yield strength of a porous material when the porosity is not high (Weng, 1984; Qiu and Weng, 1993).

We have also used the theory to calculate the compressive stress–strain relations of this TiO_2 at six selected grain sizes: $d = 10$ nm, 16 nm, 28 nm, 62 nm, 222 nm and 20 μm, at both porosity levels. The results are displayed in Fig. 4. The increase of flow stress as the grain size enters into the nano-meter range is evident (it was from

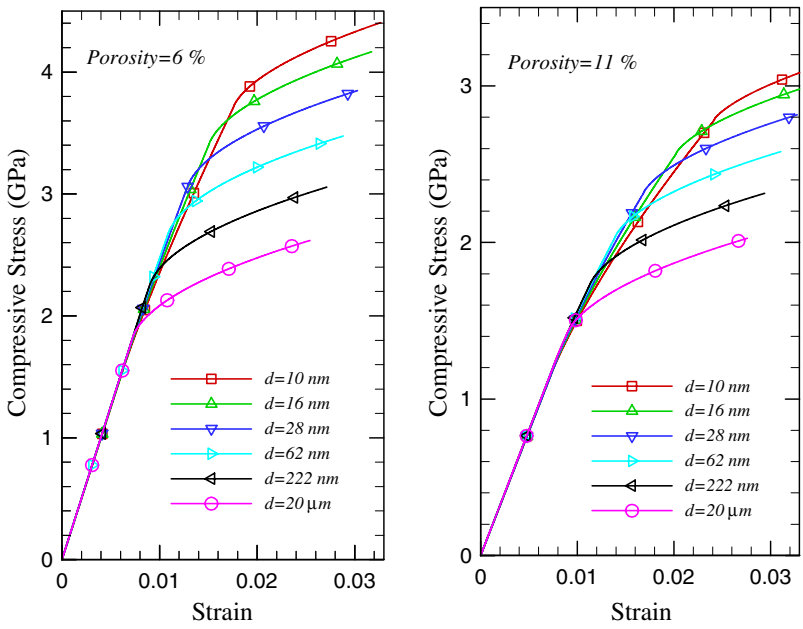

Fig. 4. Calculated compressive stress–strain relations as grain size decreases from 20 μm to 10 nm at tow porosity levels: (a) $c_{\text{pore}} = 6\%$ and (b) $c_{\text{pore}} = 11\%$.

these curves that the compressive yield stresses at 0.2% plastic strain displayed in Fig. 3 were obtained). As the porosity increased from 6% to 11%, the flow stress also decreased. Some crossover of the curves between 10 and 16 nm was also observed; this was due to an earlier yielding in the grain-boundary phase with smaller grain size. At these two levels of porosity, the compressive yield strength and overall response of the nano-grained ceramic remain very hard.

In a multiphase ceramic such as the 3-phase system synthesized by Kim et al. (2001), some phase could undergo plastic deformation whereas others may deform only elastically. The presence of second elastic phases can affect both the compressive yield strength and the overall stress–strain relation of a nano-ceramic composite. In order to shed some light on such an effect, we have made calculations for the same TiO_2 with 6% porosity, but this time with the artificial introduction of another elastic phase whose moduli differ from those of the host TiO_2 grains. The results of compressive yield strength are shown in Fig. 5. Here in the inset E_{plastic} means the Young's modulus of the plastic grains (i.e. the host TiO_2 grains), E_{elastic} means the Young's modulus of this artificially introduced elastic grains, and c_{elastic} its volume concentration (which is at the expense of the TiO_2 host grains as the porosity and grain-boundary concentrations were taken to be fixed in calculations). The first curve with $E_{\text{plastic}} = 281$ GPa and $c_{\text{elastic}} = 0$ is exactly the middle curve in Fig. 3. The other three curves were calculated with $c_{\text{elastic}} = 10\%$, one with the same elastic modulus, one stiffer at $E_{\text{elastic}} = 600$ GPa and another softer at $E_{\text{elastic}} = 100$ GPa. The one with the same Young's modulus (but deforms only elastically) has a slightly higher level of compressive yield strength than

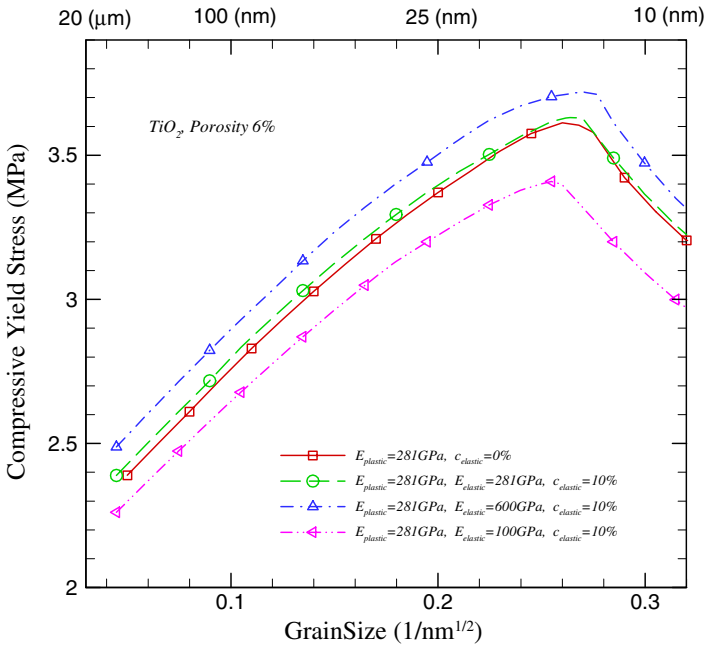

Fig. 5. Effects of a second elastic phase on the compressive yield stress of a nano-TiO_2.

the host system. The other two, on the other hand, showed a marked increase or decrease of the strength even with only 10% of concentration.

The corresponding compressive stress–strain relations of these three ceramic composites are depicted in Fig. 6, each at three selected grain levels $d = 10$ nm, 100 nm, and 20 μm. In each case the grain size is seen to play a major role. The influence of the second-phase stiffness on the overall compressive behavior is also significant.

Before we close, let us return to the TiO_2 we examined earlier, to uncover the possible influence of grain-boundary thickness on its compressive yield strength. As mentioned earlier, hydrogen probe on the grain-boundary thickness by Mütschele and Kirchheim (1987), and Kirchheim et al. (1988) suggested a range of 0.5–1.5 nm, and recent molecular dynamic simulations also indicated that the grain-boundary thickness was not sensitive to the grain size (Schiøtz, 2003). Chokshi et al. (1989) suggested the value of 1 nm for Cu and Pd. The results in Figs. 3–6 have all been calculated taking $\delta = 1$ nm. But in order to shed some light on the effect of grain-boundary thickness, we have made two additional calculations using $\delta = 0.8$ and 1.2 nm. The results for the compressive yield strength are shown in Fig. 7, at the porosity of 6%. These three curves indicate that, in the coarse grain range, grain-boundary thickness has no effect on the compressive yield strength, but smaller grain-boundary thickness would increase the compressive yield strength in the nano-meter range. The critical grain size also increases with increasing grain-boundary thickness. The basic characteristics of grain-size dependence of the compressive yield strength, however, are not altered by the grain-boundary thickness.

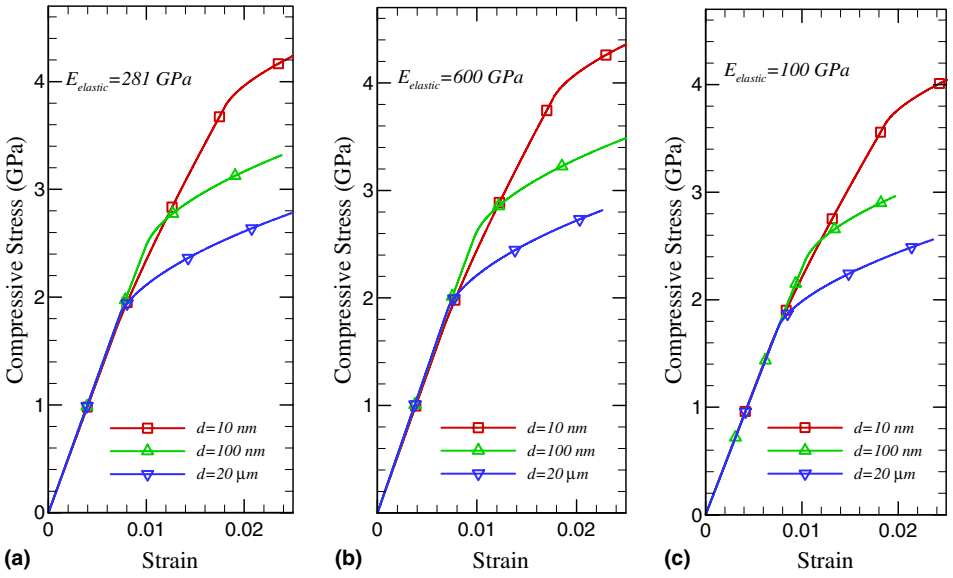

Fig. 6. Calculated compressive stress–strain relations at three different grain sizes when the elastic phase has: (a) the same, (b) stiffer, and (c) softer Young's modulus than TiO_2.

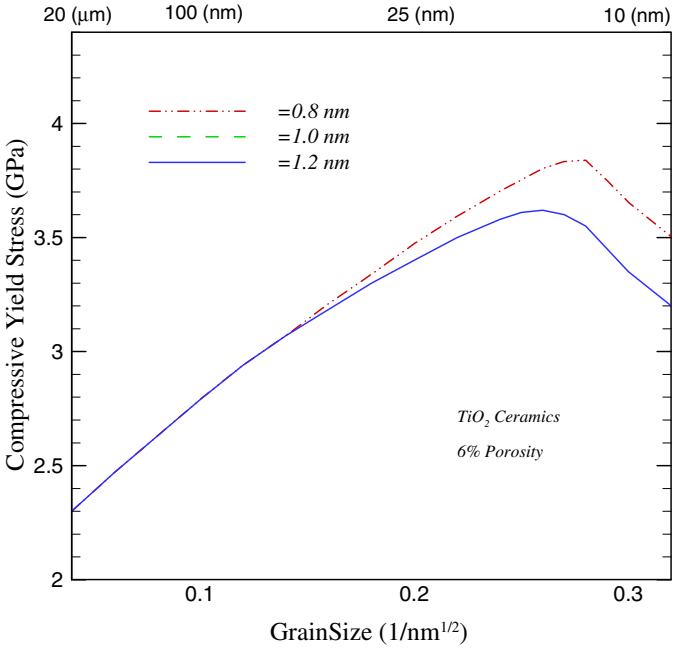

Fig. 7. Effect of the grain-boundary thickness on the compressive yield stress of TiO_2.

6. Concluding remarks

In an effort to provide a theoretical basis for the effects of porosity, grain size, and second elastic phases on the compressive yield strength of nano-grained ceramics, we have developed a composite-based model to examine the overall elastoplastic behavior of such materials. Both the grains and the grain boundary are allowed to have plastic deformation, with the elastic grains represented by a very high yield stress. A generalized self-consistent scheme is developed to determine the stress and strain state of the collective grains of each phase and that of the grain boundary, and a direct self-consistent scheme is used to determine the strain state of the pores. Under a given external stress, the overall strain of the composite is then determined by the weighted mean of the strains of these constituent phases. The overall secant bulk and shear moduli of the composite are then calculated, and used in the generalized, and the direct, self-consistent schemes for self-consistency. This procedure allows one to calculate the overall stress–strain relation and the compressive yield strength of the composite as a function of volume fractions of each constituent phase and their respective volume concentrations as the grain size decreases from the coarse-grained to the nano-grained regime. Through this scheme the effect of second elastic phases on the compressive yield strength of the nano-ceramics can also be evaluated.

The theory has been applied to study the basic characteristics of compressive yield strength of a nano-TiO_2 as its grain size decreases. It was found that the yield strength continues to increase with decreasing grain size within this range. Porosity was also found to play a significant role in reducing the compressive yield strength, but the increase of flow stress with decreasing grain size appears to follow two parallel paths at these two porosity levels. The theory further predicted the existence of a critical grain size below which the compressive yield strength began to decrease. This critical equicohesive grain size, which marks the maximum, optimal compressive strength of a ceramic, occurs at the nano-meter range.

The influence of a second elastic phase on the compressive yield strength of TiO_2 has also been investigated with an idealized composite system. The grains of this second phase could be stiffer, equal, or softer in its Young's modulus than that of TiO_2 grains, and it was found that such elastic heterogeneity has a significant effect on the compressive yield strength even at a relative low volume concentration of 10%. This suggests that second phases in a nano-ceramic composite not only could serve to suppress the grain growth but also could help improve the compressive yield strength and hardness of the nano-grained ceramics.

Acknowledgements

This work was sponsored by the Army Research Laboratory (ARMAC-RTP) and was accomplished under the ARMAC-RTP Cooperative Agreement Number DAAD19-01-2-0004. The views and conclusions contained in this document are those of the authors and should not be interpreted as representing the official

policies, either expressed or implied, of the Army Research Laboratory or the US Government. The US Government is authorized to reproduce and distribute reprints for Government purposes notwithstanding any copyright notation hereon.

Appendix A

Parameters $\bar{a}_1$, $\bar{a}_2$, $\bar{b}_1$ and $\bar{b}_2$:

$$\begin{Bmatrix} \bar{a}_1 \\ \bar{a}_2 \end{Bmatrix} = [\bar{K}_1]^{-1}_{2\times2}\left([\bar{F}_1]_{2\times2}\begin{Bmatrix} \bar{d}_3 \\ \bar{d}_4 \end{Bmatrix} + \frac{1}{2\mu^{s}_{c}}\begin{Bmatrix} 1 \\ 1 \end{Bmatrix}\right),$$

$$\begin{Bmatrix} \bar{b}_1 \\ \bar{b}_2 \\ \bar{b}_3 \\ \bar{b}_4 \end{Bmatrix} = [\bar{G}]^{-1}_{4\times4}[\bar{H}]_{4\times2}\begin{Bmatrix} \bar{a}_1 \\ \bar{a}_2 \end{Bmatrix},$$

where

$$\begin{Bmatrix} \bar{d}_3 \\ \bar{d}_4 \end{Bmatrix} = [\bar{P}]^{-1}_{2\times2}\left(\frac{1}{2\mu^{s}_{gb}}\begin{Bmatrix} 1 \\ 1 \end{Bmatrix} - \frac{1}{2\mu^{s}_{c}}[\bar{K}_2]_{2\times2}[\bar{K}_1]^{-1}_{2\times2}\begin{Bmatrix} 1 \\ 1 \end{Bmatrix}\right),$$

$$[\bar{P}]_{2\times2} = [\bar{K}_2]_{2\times2}[\bar{K}_1]^{-1}_{2\times2}[\bar{F}_1]_{2\times2} - [\bar{F}_2]_{2\times2},$$

$$[\bar{K}_1]_{2\times2} = [\bar{E}_1]_{2\times4}[\bar{G}]^{-1}_{4\times4}[\bar{H}]_{4\times2},$$

$$[\bar{K}_2]_{2\times2} = [\bar{E}_2]_{2\times4}[\bar{G}]^{-1}_{4\times4}[\bar{H}]_{4\times2},$$

and

$$[\bar{E}_1]_{2\times4} = \begin{bmatrix} 1 & -\frac{6\nu^{s}_{gb}}{1-2\nu^{s}_{gb}} & 3 & \frac{5-4\nu^{s}_{gb}}{1-2\nu^{s}_{gb}} \\ 1 & -\frac{7-4\nu^{s}_{gb}}{1-2\nu^{s}_{gb}} & -2 & 2 \end{bmatrix},$$

$$[\bar{E}_2]_{2\times4} = \begin{bmatrix} 1 & \frac{3\nu^{s}_{gb}}{1-2\nu^{s}_{gb}} & -12 & -\frac{2(5-\nu^{s}_{gb})}{1-2\nu^{s}_{gb}} \\ 1 & -\frac{7+2\nu^{s}_{gb}}{1-2\nu^{s}_{gb}} & 8 & \frac{2(1+\nu^{s}_{gb})}{1-2\nu^{s}_{gb}} \end{bmatrix},$$

$$[\bar{F}_1]_{2\times2} = \begin{bmatrix} 3 & \frac{5-4\nu^{s}_{c}}{1-2\nu^{s}_{c}} \\ -2 & 2 \end{bmatrix},$$

$$[\bar{F}_2]_{2\times2} = \begin{bmatrix} -12 & \frac{2(5-\nu^{s}_{c})}{1-2\nu^{s}_{c}} \\ 8 & \frac{2(1+\nu^{s}_{c})}{1-2\nu^{s}_{c}} \end{bmatrix}\frac{\mu^{s}_{c}}{\mu^{s}_{gb}},$$

$$[\bar{G}]_{4\times4}=\begin{bmatrix} 1 & -\frac{6\nu^s_{gb}c_g^{2/3}}{1-2\nu^s_{gb}} & \frac{3}{c_g^{5/3}} & \frac{5-4\nu^s_{gb}}{(1-2\nu^s_{gb})c_g} \\ 1 & -\frac{(7-4\nu^s_{gb})c_g^{2/3}}{1-2\nu^s_{gb}} & -\frac{2}{c_g^{5/3}} & \frac{2}{c} \\ 1 & \frac{3\nu^s_{gb}c_g^{2/3}}{1-2\nu^s_{gb}} & -\frac{12}{c_g^{5/3}} & -\frac{2(5-\nu^s_{gb})}{(1-2\nu^s_{gb})c_g} \\ 1 & -\frac{(7+2\nu^s_{gb})c_g^{2/3}}{1-2\nu^s_{gb}} & \frac{8}{c_g^{5/3}} & \frac{2(1+\nu^s_{gb})}{(1-2\nu^s_{gb})c_g} \end{bmatrix},$$

$$[\bar{H}]_{4\times2}=\begin{bmatrix} 1 & -\frac{6\nu^s_g}{1-2\nu^s_g} \\ 1 & -\frac{7-4\nu^s_g}{1-2\nu^s_g} \\ \frac{\mu^s_g}{\mu^s_{gb}} & \frac{3\nu^s_g}{1-2\nu^s_g}\frac{\mu^s_g}{\mu^s_{gb}} \\ \frac{\mu^s_g}{\mu^s_{gb}} & -\frac{7+2\nu^s_g}{1-2\nu^s_g}\frac{\mu^s_g}{\mu^s_{gb}} \end{bmatrix}.$$

References

Averback, R.S., Höfler, H.J., Hahn, H., Logas, J.C., 1992. Sintering and grain growth in nanocrystalline ceramics. Nanostruct. Mater. 1, 173–178.

Berveiller, M., Zaoui, A., 1979. An extension of the self-consistent scheme to plastically-flowing polycrystals. J. Mech. Phys. Solids 26, 325–344.

Birringer, R., Gleiter, H., Klein, H.-P., Marquardt, P., 1984. Nanocrystalline materials: an approach to a novel solid structure with gas-like disorder? Phys. Lett. 102A, 365–369.

Budiansky, B., 1995. On the elastic moduli of some heterogeneous materials. J. Mech. Phys. Solids 13, 223–227.

Chokshi, A.H., Rosen, A., Karch, J., Gleiter, H., 1989. On the validity of the Hall–Petch relationship in nanocrystalline materials. Script. Metall. 23, 1679–1684.

Christensen, R.M., Lo, K.H., 1979. Solutions for effective shear properties in three phase sphere and cylinder models. J. Mech. Phys. Solids 27, 315–330.

Donovan, P.E., 1989. A yield criterion for Pd40Ni40P20 metallic glass. Acta Metall. 37, 445–456.

Drucker, D.C., 1950. Some implications of work hardening and ideal plasticity. Q. Appl. Math. 7, 411–418.

Eshelby, J.D., 1957. The determination of the elastic field of an ellipsoidal inclusion, and related problems. Proc. R. Soc. London A 241, 376–396.

Fougere, G.E., Weertman, J.R., Siegel, R.W., Kim, S., 1992. Grain-size dependent hardening and softening of nanocrystalline Cu and Pd. Scripta Metall. Mater. 26, 1879–1883.

Gleiter, H., 2000. Nanostructured materials: basic concepts and microstructure. Acta Mater. 48, 1–29.

Guermazi, M., Höfler, H.J., Hahn, H., Averback, R.S., 1991. Temperature dependence of the hardness of nanocrystalline titanium oxide. J. Am. Ceram. Soc. 74, 2672–2674.

Hahn, H., Averback, R.S., 1991. Low-temprature creep of nanocrystalline titanium (IV) oxide. J. Am. Ceram. Soc. 74, 2918–2921.

Hill, R., 1965a. Continuum micro-mechanics of elastoplastic polycrystals. J. Mech. Phys. Solids 13, 89–101.

Hill, R., 1965b. A self-consistent mechanics of composite materials. J. Mech. Phys. Solids 13, 213–222.

Höfler, H.J., Averback, R.S., 1990. Grain growth in nanocrystalline TiO_2 and its relation to Vickers hardness and fracture toughness. Script Metall. Mater. 24, 2401–2406.

Hu, G.K., 1996. A method of plasticity for general aligned spheroidal void or fiber-reinforced composites. Int. J. Plasticity 12, 439–449.

Huang, Y., Hu, K.X., Wei, X., Chandra, A., 1994. A generalized self-consistent mechanics method for composite materials with multiphase inclusions. J. Mech. Phys. Solids 42, 491–504.

Jiang, B., Weng, G.J., 2003. A composite model for the grain-size dependence of yield stress of nanograined materials. Metall. Mater. Trans. A 34, 765–772.

Karch, J., Birringer, R., Gleiter, H., 1987. Ceramics ductile at low temperature. Nature 330, 556–558.

Kim, B.-N., Hiraga, K.K., Morita, K., Sakka, Y., 2001. A high-strain-rate superplastic ceramic. Nature 413, 288–291.

Kirchheim, R., Mütschele, T., Kieninger, W., 1988. Hydrogen in amorphous and nanocrystalline metals. Mater. Sci. Eng. 99, 457–462.

Lu, K., Wei, W.D., Wang, J.T., 1990. Microhardness and fracture properties of nanocrystalline Ni–P alloy. Scripts Metall. Mater. 24, 2319–2323.

McClintock, F.A., Argon, A., 1966. Mechanical Behavior of Materials. Addison-Wesley, New York.

Mütschele, T., Kirchheim, R., 1987. Hydrogen as a probe for the average thickness of a grain boundary. Script. Metall. 21, 1101–1104.

Ponte Castañeda, P., 1991. The effective mechanical properties of nonlinear isotropic composites. J. Mech. Phys. Solids 39, 45–71.

Qiu, Y.P., Weng, G.J., 1992. A theory of plasticity for porous materials and particle-reinforced composites. J. Appl. Mech. 59, 261–268.

Qiu, Y.P., Weng, G.J., 1993. Plastic potential and yield function of porous materials with aligned and randomly oriented spheroidal voids. Int. J. Plasticity 9, 271–290.

Sanders, D.G., Eastman, J.A., Weertman, J.R., 1997a. Elastic and tensile behavior of nanocrystalline copper and palladium. Acta mater. 45, 4019–4025.

Sanders, D.G., Youngdahl, C.J., Weertman, J.R., 1997b. The strength of nanocrystalline metals with and without flaws. Mater. Sci. Eng. A 234-236, 77–82.

Schiøtz, J. Private communication, 2003.

Schiøtz, J., Di Tolla, F.D., Jacobsen, K.W., 1998. Softening of nanocrystalline metals at very small grain sizes. Nature 39, 561–563.

Schiøtz, J., Vegge, T., Di Tolla, F.D., Jacobsen, K.W., 1999. Atomic-scale simulations of the mechanical deformation of nanocrystalline metals. Phys. Rev. B 60, 11971–11983.

Suquet, P., 1995. Overal properties of nonlinear composites: a modified secant moduli theory and its link with Ponte Castañeda's nonlinear variational procedure. C.R. Acad. Des Sci. 320 (Ser. IIb), 563–571.

Tabor, D., 1951. The Hardness of Metals. Oxford University Press, London.

Talbot, D.R.S., Willis, J.R., 1985. Variational principles for inhomogeneous nonlinear media. IMA J. Appl. Math. 35, 39–54.

Tandon, G.P., Weng, G.J., 1988. A theory of particle-reinforced plasticity. J. Appl. Mech. 55, 126–135.

Van Swygenhoven, H., Spaczer, M., Caro, A., 1999. Microscopic description of plasticity in couputer generated metallic nanophase samples: a comparison between Cu and Ni. Acta Mater. 47, 3117–3126.

Weertman, J.R., Farkas, D., Hemker, K., Kung, H., Mayo, M., Mitra, R., Van Swygenhoven, H., 1999. Structure and mechanical behavior of bulk nanocrystalline materials. MRS Bull. 24, 44–50.

Weng, G.J., 1983. A micromechanical theory of grain-size dependence in metal plasticity. J. Mech. Phys. Solids 31, 193–203.

Weng, G.J., 1984. Some elastic properties of reinforced solids, with special reference to isotropic ones containing spherical inclusions. Int. J. Eng. Sci. 22, 845–856.

Willis, J.R., 1991. On methods for bounding the overall properties of nonlinear composites. J. Mech. Phys. Solids 39, 73–86.

Yamakov, V., Wolf, D., Phillpot, S.R., Gleiter, H., 2002. Grain-boundary diffusion creep in nanocrystalline palladium by molecular dynamics simulation. Acta Mater. 50, 61–73.